MODIFICATION OF AZ91 MAGNESIUM ALLOY FOR HIGH TEMPERATURE APPLICATION

A thesis submitted in partial fulfillment of the requirement for the degree of

Master of Technology

(Dual Degree)

In

Metallurgical and Materials Engineering

By

Punit Kumar

[Roll No.: 710MM1093]

Department of Metallurgical and Materials Engineering

National Institute of Technology, Rourkela

Odisha-769008, India

May 2015

Department of Metallurgical and Materials Engineering

National Institute of Technology, Rourkela

Odisha-769008, India

Phone: 0661 2462550

CERTIFICATE

This is to certify that the thesis entitled "**Modification of AZ91 Magnesium Alloy for High Temperature Application**" is being submitted by **Mr. Punit Kumar** for the award of the degree of ***Master of Technology*** in **Metallurgical and Materials Engineering** at the Department of Metallurgical and Materials Engineering, National Institute of Technology, Rourkela, Orissa, India is a record of bonafide research work carried out by him under my guidance and supervision.

Dr. Ashok Kumar Ray
Chief Scientist, Material Science
and Technology Division
CSIR-National Metallurgical Laboratory
Jamshedpur-831007

Dr. Ashok Kumar Mondal
Department of Metallurgical and
Materials Engineering
National Institute of Technology
Rourkela-769008

ACKNOWLEDGEMENT

"If I have seen the further it is by standing on the shoulders of giants". That's the first thing that came to my mind when I started writing my thesis. The things I have learnt and experience I have gained from my project work is invaluable. The words may fall short to thank you all for your support and guidance.

I like to express my sincere gratitude to my project mentor, Dr. Ashok Mondal. I feel fortunate to have him as my mentor as he was always there to guide me through all the problems and inspire me to achieve more.

I wish to thank my co-supervisor Dr. Ashok Kumar Ray for his untiringly help in the project, support for technical work and valuable suggestions. I would like to say that things that I have learnt from you will always guide me through my life. I am very much grateful to Dr. Sandip Ghosh Chowdhury for his help in Microstructure evaluation, XRD analysis and his valuable suggestions during my project.

I thank Dr. S.C. Mishra HOD of Metallurgical and Materials Engineering of NIT Rourkela, Dr. S. Tarafdar HOD of MST Division of CSIR-NML Jamshedpur for providing me the exclusive opportunity to carry out this project at NIT Rourkela and CSIR-NML Jamshedpur. I wish to thank A.K.S. Bankoti, Hrishikesh Shastri, and Pranab Bhale for their help during casting and other valuable suggestions. My sincere thanks to Vinod Kalindi, Ankur Chatarjee, P.S. Manornjan Jena, Navin Kumar for their help during creep testing and microstructural evaluation. At last a lot of thanks to my family and especially my parents for their support and love. Special thanks to my brother A. P. Ranjan for always encouraging me to achieve more.

(PUNIT KUMAR)

CONTENTS

Title page..... i

Certificate.....ii

Acknowledgement..... iii

Content.....iv

Tables.....vii

List of Figures.....viii

Abstract.....x

Chapter 1: INTRODUCTION 1

1.1 Magnesium (Mg)..... 2

1.2 AZ91 Mg alloy..... 3

1.3 Creep behavior of AZ91Mg alloy..... 5

1.4 Premise of the thesis..... 6

Chapter 2: LITERATURE SURVEY 7

2.1 Introduction.....8

2.2 Application of Mg alloys..... 9

2.3 Casting process..... 10

2.4 Major Mg alloy system..... 10

2.4.1 Alloys containing zirconium..... 11

2.4.2 Zirconium free Alloys (Mg-Al alloys).....12

2.5 AZ91 alloy (Mg-9Al-1Zn- 0.3Mn) (wt%).....12

2.6 Effect of alloying additions to AZ91 alloy..... 14

2.6.1 Ca addition.....14

2.6.2 Bi addition.....15

2.6.3 Sb addition.....16

2.6.4 Sr addition.....17

2.7 Effect of combined alloying addition to AZ91alloy.....18

2.8 Novelty of the present work.....20

Chapter 3: EXPERIMENTAL PROCEDURE 21

3.1 Work plan.....22

3.2 Fabrication of the alloys.....22

3.2.1 Melting and casting.....23

3.2.1.1 Squeeze casting of AZ91 alloy.....23

3.2.1.2 Squeeze casting of AZY910 alloy.....24

3.2.1.3 Squeeze casting of AZJ910 and AZJY9100 alloys.....24

3.3 Chemical analysis of the fabricated alloys.....25

3.4 Creep test.....26

3.5 Microstructure characterization.....27

3.5.1 X-Ray diffraction (XRD).....27

3.5.2 Optical microscopy.....27

3.5.3 Scanning electron microscopy.....28

Chapter 4: RESULTS AND DISCUSSION 29

4.1 Microstructural characterization.....30

4.1.1 Phase analysis using XRD.....30

4.1.2 Optical micrographs.....31

4.1.3 SEM micrographs..... 32

4.2 Results of creep tests.....35

4.2.1 Phase analysis after creep test.....37

4.3 Fractography..... 39

Chapter 5: CONCLUSIONS **41**

5.1 Conclusions.....42

5.2 Future scope of work..... 43

Chapter 6: REFERENCES **44**

TABLES

Table No.	Table Caption	Page No.
1.1	Mechanical properties of different Mg-Al based alloys	4
2.1	Elements and their abbreviation designation of Mg alloys	10
2.2	Effect of additions of Sr and other alloying elements to AZ91 alloy	19
3.1	Results of bulk EDX analysis from the AZY910 alloy	25
3.2	Results of bulk EDX analysis from the AZJ910 alloy	25
3.3	Results of bulk EDX analysis from the AZJY910 alloy	25
3.4	Target compositions, achieved compositions and corresponding alloy designations of squeeze-cast alloys	26
4.1	Grain size and volume fraction of the β-$Mg_{17}Al_{12}$ phase of the alloys	32

LIST OF FIGURES

Figure No.	Figure Caption	Page No.
1.1	Unit cell of Mg alloy showing slip plane and slip directions	3
1.2	Mg-Al phase diagram	4
2.1	Variation of fuel efficiency with vehicle weight	8
2.2	Use of Mg alloy in automobiles	9
2.3	Optical micrographs of AZ91 alloys: (a) with no Ca addition, (b) with 1.5 wt% Ca addition	14
2.4	SEM micrographs of the (a) AZ91 alloy and (b) AZRC91 (Ca + RE) alloys	15
2.5	(a) Creep curve of the AZ91 alloy with Sb and Si additions and (b) SEM micrograph of the crept AZ91+Si+Sb alloy	17
2.6	Optical micrographs of the (a) AZ91, (b) AZ91-1Y-0.5Ca, (c) AZ91-1Y-1.0Ca, (d) AZ91-1Y-1.5Ca alloys	18
3.1	Detail work plan	22
3.2	Bottom pouring type stir casting furnace with squeeze casting facility	23
3.3	Squeeze cast AZY910 alloy	24
3.4	(a) Schematic of creep test specimen and, (b) Machined creep test specimen	26
3.5	Photograph of the creep testing machine	27
4.1	XRD patterns of the squeeze-cast (a) AZ91D, (b) AZY910, (c) AZJ910, and (d) AZJY9100 alloys	30

4.2	Optical micrographs of the squeeze-cast (a) AZ91D, (b) AZJ910, (c) AZY910, and (d) AZJY9100	31
4.3	SEM micrographs of the squeeze-cast (a) AZ91D, (b) AZJ910, (c) AZY910, and (d) AZJY9100 alloys	33
4.4	Variation of Al content (wt%) across the β-$Mg_{17}Al_{12}$ present along the grain boundary	33
4.5	EDS elemental mapping taken from the AZJY9100 alloy for Mg, Al, Zn, Sb and Mn	34
4.6	Creep curves of the alloys (a) AZ91, (b) AZJ910, (c) AZY910, and (d) AZJY9100 tested at 70MPa and 175°C	35
4.7	(a) Comparison of all the creep curves, (b) Steady state creep rate of the alloys; (c) results of line scan taken across β-$Mg_{17}Al_{12}$ phase in AZJY9100 alloy, and (d) SEM Micrograph of the creep cavity formed in the AZJY9100 alloy.	37
4.8	XRD pattern of the (a) as-cast and (b) creep tested AZJY9100 alloy	38
4.9	Elemental mapping taken from the AZJY9100 showing Sb distribution	38
4.10	SEM fractographs of the creep tested (a) AZ91, (b) AZJ910, (c) AZY910, and (d) AZJY9100 alloys	39

ABSTRACT

In recent years, the lightweight requirement has become crucial in aerospace and automobile application. Mg alloys provide an excellent alternative to conventional structural metals and alloys as it has the highest specific strength. Mg-alloy AZ91 (Mg-9Al-0.8Zn-0.2Mn) is the most favored alloy, being used in approximately 90% of all magnesium cast products. It has good castability, excellent room temperature (RT) mechanical properties and has low cost compared to other Mg-alloys. However, above 120°C its mechanical properties deteriorate because of the low softening temperature of same β-$Mg_{17}Al_{12}$ which provides it better RT mechanical properties. The present study is an attempt to improve the creep strength of AZ91 through the addition of alloying elements which form thermally stable intermetallics and pins the β-$Mg_{17}Al_{12}$. The effects of individual and combined additions of Sb and Sr on the microstructure and creep properties of squeeze-cast Mg-AZ91 alloy have been investigated. For comparison, the same has also been studied on the as-cast AZ91 alloy without any addition. The results indicate that individual and combined addition of Sr and Sb refine the grain size, β-$Mg_{17}Al_{12}$ phase, and it affects the dynamic precipitation of β-$Mg_{17}Al_{12}$ during creep. All the alloys have been creep tested at a temperature of 175°C and a stress level of 70 MPa. The lowest steady state creep rate is obtained in the AZ91 alloy pertaining combined addition of both Sb and Sr owing to the presence of relatively lower amount of β-$Mg_{17}Al_{12}$ phase and high melting point intermetallics Mg_3Sb_2 and Al_4Sr phase.

Chapter 1

INTRODUCTION

1.1 Magnesium (Mg)

Use of modern features and extra safety measures in automobiles has caused an increase in weight that ultimately results in higher fuel consumption. Higher fuel consumption increases the pollution through more emission of CO_2 [1]. In recent years, research and development of magnesium alloys have become more prominent because of the lightweight requirement in the automotive industry and aerospace industry, which can save our limited fuel resources and also decrease environmental pollution. Magnesium with the density (1.74 gm/cc) is the lightest structural metal. Magnesium is also one of the most abundant elements as 6 million tonnes of Mg could be found in 1 cubic mile of sea water. Initially in 1916 Mg was produced in Germany but it could not catch market because of lack of demand. During the second world was Mg production increased up to 237000 tonnes because of its newly found applications in the defense industries. The production of Mg decreased after world war but in the recent year it has again got attention due to increasing demand in automobile industries. Mg production has grown with 16% rate in last decade, and it has been predicted that it will grow with 11.5% rate in next decade. Still it has the potential to grow in new sectors, and it has not reached up to its potential. The reason behind this is the knowledge of Mg and its alloys have not been researched up to a large extent as other metals like Al. But nowadays a lot of researchers are working on the Mg-Alloy, which will ultimately unlock the potential use of magnesium in new areas coming days.

Mg has hexagonal crystal structure with c/a ratio 1.6236 which is very close to ideal value 1.633. Fig.1.1 shows the atomic plane and direction of Mg unit cell. Mg has low ductility at 30°C because only three slip system is active but at higher temperature prismatic planes and pyramidal slip planes also becomes active causing higher ductility.

At room temperature, only three slip systems are active, all parallel to the basal plane (0001) [2]. All the slip planes and direction is listed in Figure 1.1.

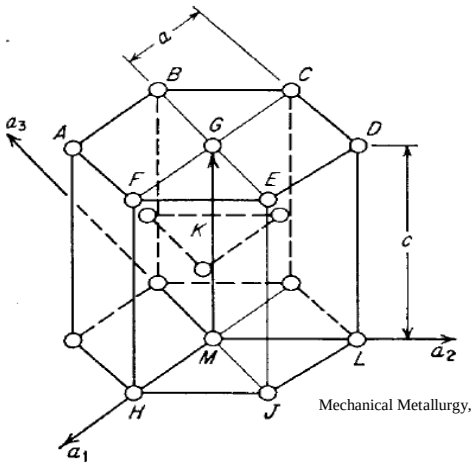

Mechanical Metallurgy, G.E. Dieter

Basal plane (0001)-ABCDEF

Prism plane (10-10)-FEJH

Pyramidal planes-

Type I, Order 1 (10-11)-GHJ

Type I, Order 2 (10-12)-KJH

Type II, Order 1 (11-21)-GHL

Type II, Order 2 (11-22)-KHL

Figure 1.1 Unit cell of Mg-alloy showing slip planes and slip directions

1.2 AZ91 Mg alloy

Mg forms solid solution with a range of elements i.e. Zn, Al, Sn, Ce, Ag, Zr, Th, Li, etc. It can also provide a good combination of castablity and mechanical properties with a right combination of alloying constituents. Aluminum as an alloying addition has found the most favor because it improves castability of the alloy by reducing the freezing range. It provides strengthening by solid solution and precipitation of the intermetallic phase ($Mg_{17}Al_{12}$). Figure 1.2 Shows the Mg-Al binary phase diagram that indicates the presence of $Mg_{17}Al_{12}$ that precipitates at room temp.

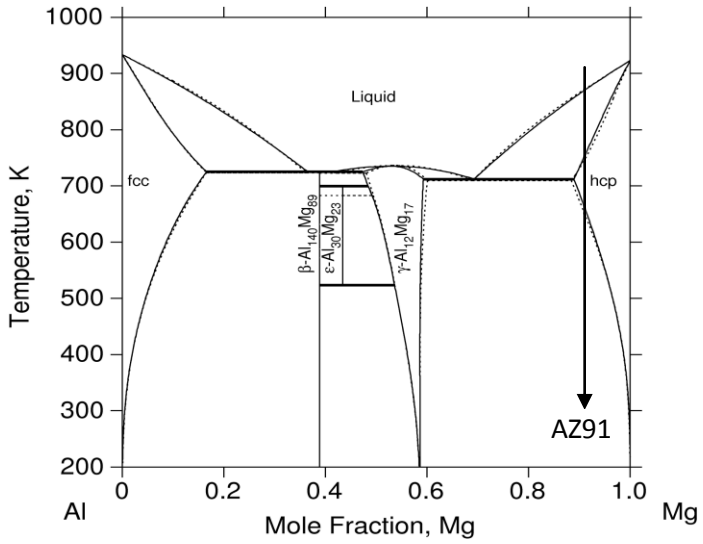

Figure 1.2 Mg-Al phase diagram

Mg-alloy AZ91 (Mg-9Al-0.8Zn-0.2Mn) is the most favored alloy, being used in approximately 90% of all magnesium cast products. It provides excellent castablity, excellent room temperature (RT) mechanical properties and it is available at low cost compared to other Mg-alloys. AZ91D Die cast alloy shows very good mechanical properties. Table.2 [3] shows the mechanical properties of AZ91 compared to other Mg-Alloy.

Table 1.1 Mechanical properties of different Mg-Al based alloys [3]

Alloy	Casting Process	Yield Strength (MPa)	Tensile Strength (MPa)	Elongation (%)
AZ91	Die Cast	150	230	3
AM60	Die Cast	115	205	6
AS41	Die Cast	150	220	4
AS21	Die Cast	130	240	9
AE41	Die Cast	103	234	15

1.3 Creep behavior of AZ91 Mg alloy

Creep occurs in the material when it exposed to high temperature and load for a long period. So, creep is a time depended deformation which takes place even at constant stress/load level below the yield strength of any material. Creep mechanism of material has been classified into two type dislocation creep and diffusion creep based on temperature and stress applied. Dislocation creep has been further subdivided into two groups' dislocation glide and climb. Diffusion creep has been also subdivided into different groups mainly grain boundary sliding, boundary diffusion (Nabarro-Herring creep) and bulk diffusion (Coble creep) [2]. Elaborate research work is currently going on the creep properties of AZ91. It has been confirmed by many research work that dislocation climb is primary creep mechanism at initial stress level 20-100 MPa in the temperature range 100-300°C. However, some literature proposed a grain boundary sliding mechanism at the low stress levels of 20-40 MPa [4].

AZ91 alloy shows its structure is not stable during creep exposure in both die cast and gravity cast alloy [5, 6]. However, die cast alloy show higher instability because of the presence of supersaturated α-Mg along the grain boundary that precipitate during creep. Dynamic precipitation has been established in many works of literatures, and it mostly suggests that discontinuous precipitation deteriorates the creep strength. The dynamic precipitation has been confirmed in some papers reported, but its influence on creep behavior is still inconclusive. Continuous precipitation provides higher creep strength as suggested in paper [5]. Higher creep rate of AZ91 could also be contributed to the higher diffusivity of Al in Mg.

1.4 Premise of the thesis

Above 120°C the mechanical properties of AZ91 alloy deteriorate because of the low softening temperature of same β-phase which provides it better RT mechanical properties. The β-phase ($Mg_{17}Al_{12}$) has melting temperature 437°C, which makes it softer at even 100-120°C and this results in grain boundary sliding at high temperature [7]. Because of this problem the AZ91 has been refrained from its use in powertrain application. It is believed that AZ91 has not been used to its potential. A lot of alloys have been developed using Rare Earth addition, but the addition of RE makes these alloys costly. Present work is targeted to develop cheap and creep resistant alloy through addition of alloying element other than RE.

The thesis "**Modification of AZ91 Magnesium Alloy for High Temperature Application**" is an attempt to improve the creep strength of AZ91 alloy through the addition of alloying element Sr and Sb. The effect of Sb and Sr addition on microstructure and effect of intermetallic (formed due to the addition) on creep properties are also investigated.

Chapter 2

LITERATURE SURVEY

2.1 Introduction

Today family cars like SUV and XUVs are becoming more and more popular. These XUVs weigh 20% more than earlier cars. The main reason behind the increase in weight is the higher weight of diesel engine, and additional safety features added. On the other hand today in the age of information customers are becoming more and more aware of environmental issues, this has created new challenges in automobile industries. The effect of weight on fuel efficiency could be seen in the Figure 2.1 [8].

Following the challenges for the weight reduction automobile industry has opted to use light metal and alloys like Al and Mg. These light metals and alloys have resulted in 10% decrease in weight from 1978 also considering safety [9]. Earlier Al provided a very good alternative to steel and other cast component, but to reduce weight further it is needed to find metal/alloys lighter than Al. As Mg has density 1.74 g/cc which is very much lighter compared to Al (2.7 g/cc). Mg has highest specific strength compared to Al and steel as it is lightest structural metal available. However, the consumption of Mg is still only the fraction of the consumption of steel and Al. There are several factors to it but, in the recent year use of magnesium is growing at a faster rate.

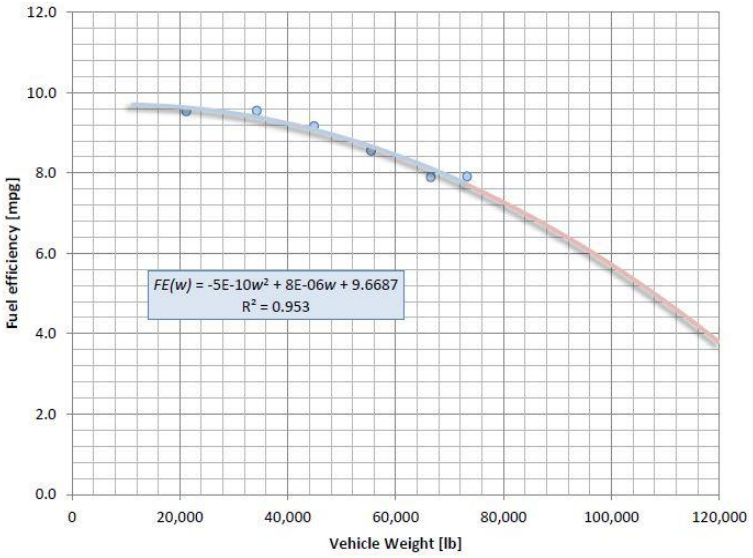

Figure 2.1 Variation of fuel efficiency with vehicle weight [8]

2.2 Application of Mg alloys

Magnesium is mostly used in automobile, aerospace and defense industries because of its high specific strength. This plays a major role in improving fuel efficiency.

In aerospace industry it is mostly used in part of the aircraft engine, landing wheel, gear housing, air frames, and seat [10]. Along with highest specific strength Mg-alloys also have good fatigue, impact toughness, and high temperature strength that is vital for aerospace application. Alloys ZE4l (Mg-4%, Zn-0.7%, Zr-1.3%), QE22 (Mg-0.7% Zr, 2.5% Nd, 2.5% Ag) and WE43 (Mg-4% Y, 3.25% Nd, 0.5% Zr) are mostly used in aerospace industries because of their high creep strength and corrosion resistance. Automobile industries are the place where Mg alloy is getting used extensively. Figure 2.2 shows some of the parts of automobile where Mg is getting used currently. But Mg alloy is still not used in the engine block and engine hood because of lack in high temperature strength.

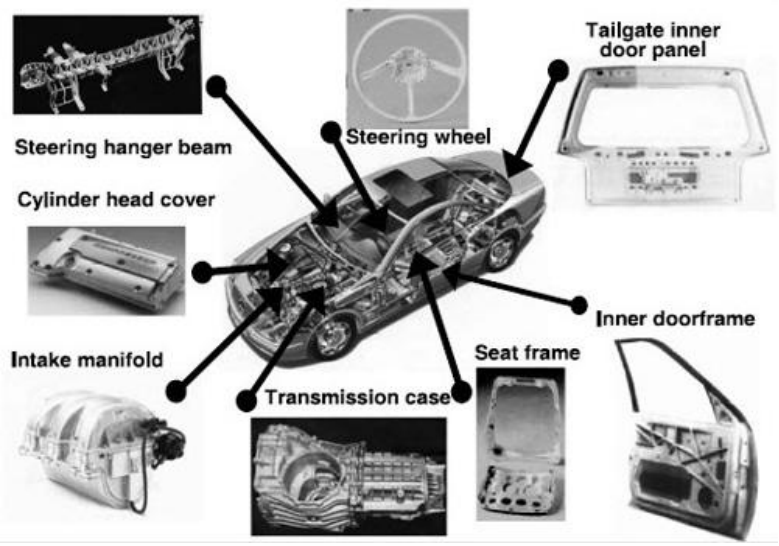

Figure 2.2 Use of Mg alloys in automobile parts

The magnesium alloy is also used in nuclear industry because it has properties like less tendency to absorb the neutron, good thermal conductivity, does not react with uranium and CO_2, even up to high temperature. Mg alloy is getting used extensively in electronic gadgets, smart phones because of its lower weight.

2.3 Casting processes

Usually, die cast process is used for casting of Mg-alloy as it has lower cost compared to other processes [11]. The addition of Al improves the castablity of Mg as Al addition results in the formation of a eutectic. Apart from die casting other casting processes like high pressure die casting, gravity casting, sand casting, and Squeeze casting process are other popular processes. AZ91, AE42, and AM60 are most common commercially used Mg-Al alloy. Rare earth element addition in alloy AE42 decreases the castablity that's why it is casted through sand casting route. Mg-Al and Mg-Al-Zn alloys show better castablity, but they show micro shrinkage when they are sand casted, but they have limited applicability above 120°C.

2.4 Major Mg alloy systems

Alloy designation of Mg alloy was standardized by ASTM (American society for testing materials); they have fixed the code (Table 2.1) for first two major alloying additions in Mg alloy.

Table 2.1 Elements and their abbreviations used for designation of Mg alloys

Element	Al	RE	Sr	Zr	Sb	Mn	Zn	Ag	Sn
Code	A	E	J	K	Y	M	Z	Q	T

The element code is used in combination according to their composition in wt% present in alloy followed by the round number.

When Mg-alloy Zr is added it acts as a very effective grain refiner but when it is added with Al, Zr loses its grain refining effect as they form intermetallics together. Based on this Mg-alloy can be classified into two categories

(I) Zirconium containing alloy

(II) Zirconium free alloys/ Al containing alloy

2.4.1 Alloys containing zirconium

Zr shows very limited solid solubility even in molten Mg (0.6%), because of this binary alloy of Mg-Zr does not have enough strength. Mg-Zn-Zr (ZK51) alloys were developed to get enough strength so that it could be used commercially. However, this alloy also shows micro crack due to shrinkage and low weldablity. But when RE (Mischmetal) is added along with Zn (EZ33) it provides very high strength and improves castablity, this finds application in aerospace industries. These alloys also show very high creep strength up to 250°C [12]. Yttrium shows very high solid solubility in Mg; this makes alloy Mg-Y age hardenable. The addition of Zr provides grain refining in alloy Mg-Y-Nd-Zr (WE54), giving WE54 very high strength even up to 300°C [13, 14]. Thorium addition in Mg alloy increases the creep strength; these alloys can be used even up to 350°C. Ternary alloy with Th and Zr has been also developed for high temperature application. Ternary compositions such as HK3l (Mg-3Th-0.7Zr) is developed for high temperature applications. Alloy with the addition of silver were developed to get high room temperature strength and creep strength [15]. QE22 (Mg-2.5Ag-ZRE-0.7Zr) alloy with addition of Ag can be used in number of aerospace applications like gear box housings, landing wheels, and as a rotor heads in helicopters.

2.4.2 Zirconium free alloys (Mg-Al alloys)

Al is most used alloying element in Mg-alloy. Almost 90% of the alloys are Mg-Al based. The alloy system Mg-Al also contains a small amount of Zn and Mn. The alloy AZ91 is mostly widely used alloy system [16]. This alloy has very good room temperature mechanical properties, and it also shows good castablity, mostly processed through die casting route. But the drawback of this alloy is the poor high temperature strength [17]. AS41, AS21 is the example of other alloy system developed with Al addition that also contains Si, which gives high creep resistance [11]. Further alloy with RE addition was developed designated as AE series with high creep strength and room temperature mechanical properties.

2.5 AZ91 alloy (Mg-9Al-1Zn-0.3Mn) (wt%)

AZ91 Mg alloy is most common alloy which is used in almost 90% of Mg cast products.

From Figure 1.2, binary phase diagram of Mg and Al, it is clear that β-$Mg_{17}Al_{12}$ intermetallic precipitation takes place. This precipitation takes place along the grain boundary to counter the interfacial energy required precipitating inside the grain. This β-$Mg_{17}Al_{12}$ enhances the room temperature mechanical properties of AZ91. However, the melting point of this intermetallic is very low (437°C). The low melting point of this intermetallic restricts the use of AZ91 alloy in powertrain application.

A lot of literature has been reported to improve the high temperature properties of AZ91 through modification in its microstructure by different alloying addition. The following few methods have been proposed in countering the problem.

I. Reduction of Al content so that β-Phase will be less in the alloy but care should be taken because Al also improves the castablity of Alloy.

II. Addition of some constituents like Si, Sr, Ca, Bi, Sb and rare earth (RE) elements which can form intermetallic with Mg and Al that have high melting point so that it will pin the grain boundary at elevated temperature and resist the grain boundary sliding.

III. Addition of some surface active elements such as Ca, Sb and Sr which can be used in the modification of β ($Mg_{17}Al_{12}$) phase, these cause reduction in the grain size, and produce fine grain boundary precipitates to improve creep resistance. They can also increase the fluidity resulting better cast ability of existing alloys.

The search of suitable alloying element could be on following constrain

I. The alloying element should show sufficient solubility in Mg at high temperature, which increases with increasing temperature so that age hardening becomes possible through precipitates from the supersaturated solution.

II. The precipitates should acquire a high Mg-content thereby increasing the volume fraction of precipitates phase thus reducing the required amount of alloying element.

III. The precipitates formed by alloying element should have a high melting point so that it does not get soften at high temperature and stop the grain boundary sliding by pinning them.

IV. The diffusion of alloying element in the alloy should be very low so that tendency to over aging, and dislocation climb gets reduced. Rare earth metals are particularly suitable, but they are very costly.

2.6 Effect of alloying additions to AZ91 alloy

2.6.1 Ca addition

Qudong et al. [18] concluded that addition of Ca to AZ91 refine the grain size and reduces the dendrite cell of β ($Mg_{17}Al_{12}$). The Ca also reacts with Al to form Al_2Ca intermetallic that is stable up to very high temperature. Impact toughness increases firstly with Ca addition but decreases finally because of reticular distribution of Al_2Ca along the cell boundaries (Figure 2.2). L. Lin et. al [19] added Ca (0.5 wt%, 1.0 wt% and 1.5 wt%, respectively) in AZ91 through die casting route. Below 0.5% ca did not show much effect on microstructure. But when Ca was increased up to 1.5 wt%, homogeneous and refined distribution of $Mg_{17}Al_{12}$ (Figure 2.2) was achieved. There was significant improvement in high temperature tensile strength. A similar result was obtained by Alan A. Luo et. al [20].

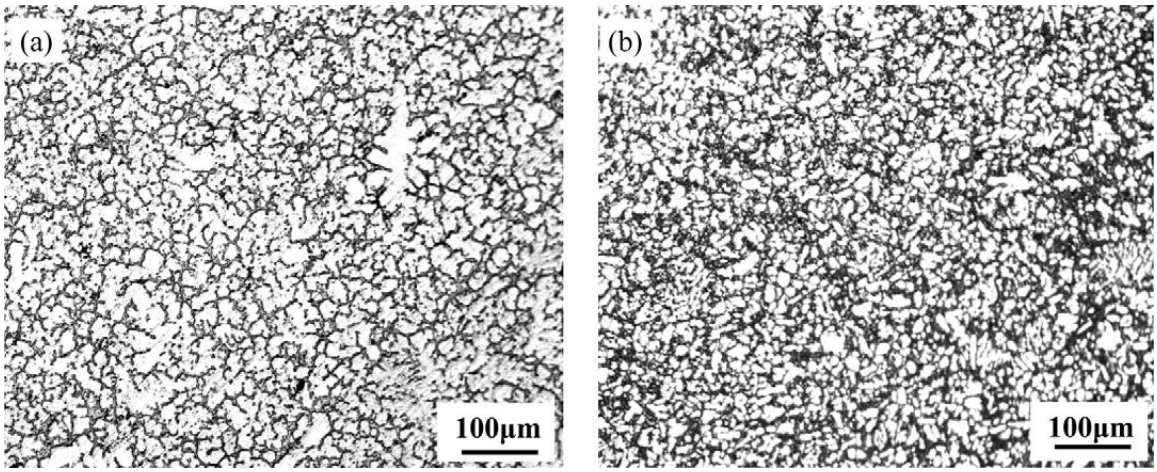

Figure 2.3 Optical micrographs of the AZ91 alloys: (a) with no Ca addition, (b) with 1.5 wt% Ca addition [19]

The addition of Ca and RE in AZ91 and its effect on creep strength was analyzed by Nami et al. [21]. It was found that creep properties of these alloys are comparable with AE42 alloy.

Ca and RE addition decreased the amount of β ($Mg_{17}Al_{12}$) (Figure 2.3) phase and also formed the intermetallics $Al_{11}RE3$ and Al_2Ca, which improved the mechanical properties significantly.

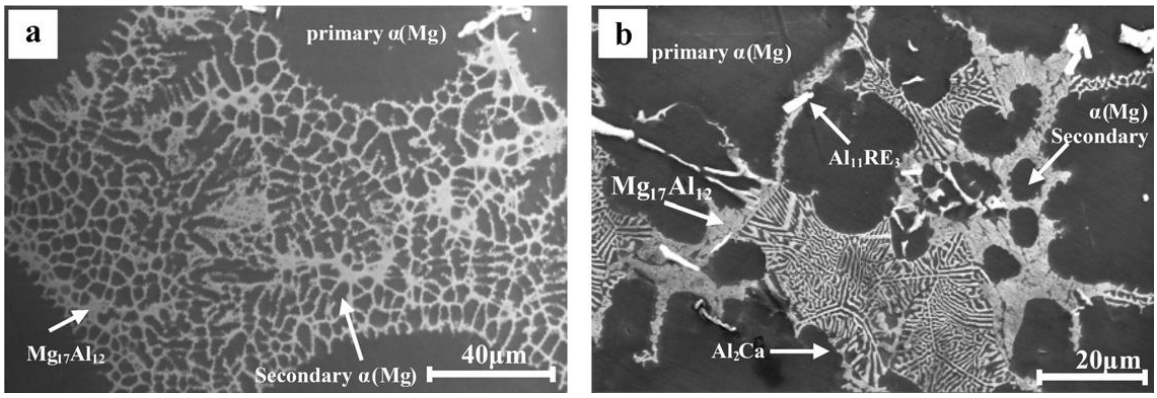

Figure 2.4 SEM micrographs of the (a) AZ91, and (b) AZRC91 (Ca + RE) alloys [21]

However, Amberger et al. [22] found that though intermetallic skeleton formed improve the creep strength of alloy but pre deformation of this alloy destroys the skeleton and leads to lower creep strength. Ca addition also decreases the castablity of AZ91, which makes it very difficult to form via. die casting route. These problems in the Ca added barred them from getting commercialized.

2.6.2 Bi addition

Bi addition in AZ91 results in decrease in the cell size of $Mg_{17}Al_{12}$ precipitation and it also decreases the grain size. Bi addition results in the formation of intermetallic Mg_3Bi with melting point 823°C. Compared to other addition like Sb and Ca, Bi shows very little improvement in creep properties. But when it is combined with Sb it shows very appreciable improvement in creep strength [23].

2.6.3 Sb addition

Sb has very low solid solubility in AZ91, because of that most of the Sb forms intermetallic with Mg. Wang et al. [24] found that Sb addition to AZ91 shows significant grain refining. The $Mg_{17}Al_{12}$ phase is also refined, and a new Mg_3Sb_2 intermetallic with melting point 1228°C is formed. Mg_3Sb_2 becomes coarser as the added amount of Sb increases. Room-temperature tensile strength, impact toughness and elongation increase first, and then decreases with the increase in Sb content as it results in coarsening of Mg_3Sb_2.

Guangyin et al. [25] concluded that Small amount of Sb additions to the AZ91 based alloys increased the creep strength and yield strength significantly. Sb addition made this alloy stable up to 200°C but caused slight decrease in ductility. The Mg_3Sb_2 intermetallic formation was confirmed that has very low thermal expansion co-efficient. The Mg_3Sb_2 structure was HCP, which is same as the α-Mg this causes the higher compatibility of Mg_3Sb_2 with α-Mg.

Srinivasan et al. [26] found that the incompatibility of the massive β-$Mg_{17}Al_{12}$ (BCC structure) in α-matrix causes the formation of cavity and cracking at the grain boundary leading to failure. The thermally stable intermetallic Mg_3Sb_2 strengthen the grain boundary and results in the formation of a greater volume of dynamic continuous precipitates causing higher creep strength (Figure 2.4).

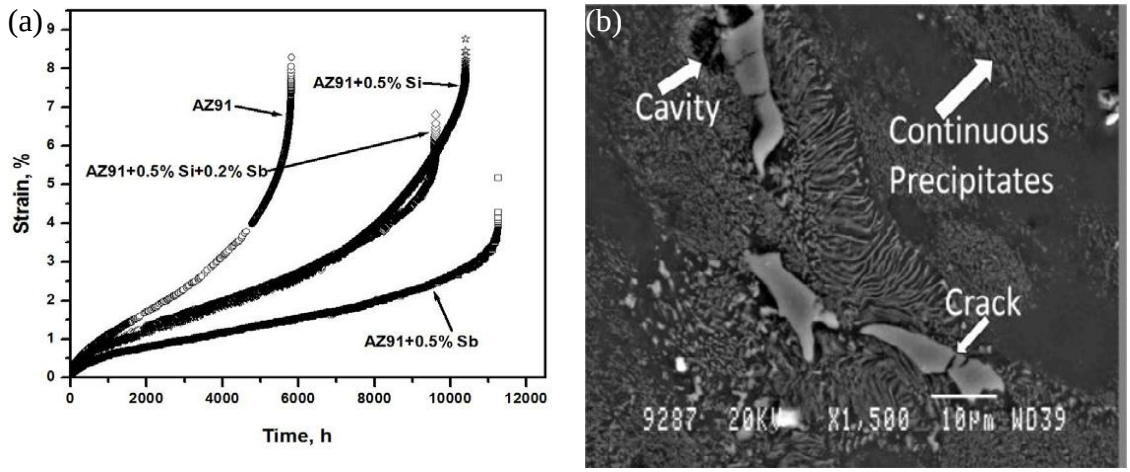

Figure 2.5 (a) Creep curve of the AZ91 alloy with Sb and Si additions and (b) SEM micrograph of the crept AZ91+Si+Sb alloy [26]

2.6.4 Sr addition

The Sr addition and its effect on creep properties have not been analyzed extensively. Present research deals with the above problem and work is targeted towards the end to generate literature.

Lee et al. [27] analyzed the Sr addition to AZ91 through squeeze casting route. By the addition of Sr in AZ91 the grain size was reduced by half compared to the base alloy. He found that the needle shape Mg-Sr presence at grain boundary makes its hard and fracture strength becomes worse than that of the AZ91 alloy, despite the considerable grain refining.

Hirai et al. [28] studied the Effects of Ca and Sr on the microstructure and creep properties. He concluded that the optimal amount of addition of the Ca and Sr were at least 1.0 and 0.5 wt%, respectively to get the maximum effect of grain refinement. The high temperature strength of these alloy also increased significantly with this addition. The grain size was refined up to 20μm this resulted in tensile strength up to 250MPa and 3% elongation. Nakaura et al. [29] also found the similar results with the addition of Ca and Sr. he reported that the addition of 0.2% Sr improved the castablity of alloy significantly.

2.7 Effect of combined alloying additions to AZ91 alloy

Srinivasan et al. [30] investigated the effect of combined addition of Si and Sb in AZ91 alloy. He investigated the effect of Sb addition on the structure of Chinese script Mg_2Si formed due to Si addition. He found that the addition of 0.2 wt% Sb change the shape of Mg_2Si and make it polygonal. Mg_2Si precipitates both at the grain boundary and inside the grain. While aging the discontinuous precipitation was suppressed because of Sb addition which caused improvement in creep strength up to 200°C (Figure 2.4). Srinivasan et al. [31] studied the effect of combined addition of Sb and Pb on the ageing behavior of AZ91 alloy. He found that the discontinuous precipitation of $Mg_{17}Al_{12}$ during ageing was suppressed significantly by Pb addition which resulted in the decrease in peak hardness of the alloy. Sb also suppressed the precipitation to a lower extent than Pb but because of hard intermetallic Mg_3Sb_2 its peak hardness did not decrease. Feng et al. [32] investigated the effect of combined addition of Ca and Y on the microstructure and mechanical properties die casting AZ91. The results show refined microstructure (Figure 2.5) due to the combined addition and formation of intermetallics Al_2Ca and Al_2Y. The ambient tensile strength and high temperature strength both improved by the addition of Y, however, Ca addition had very little effect on ambient temperature properties.

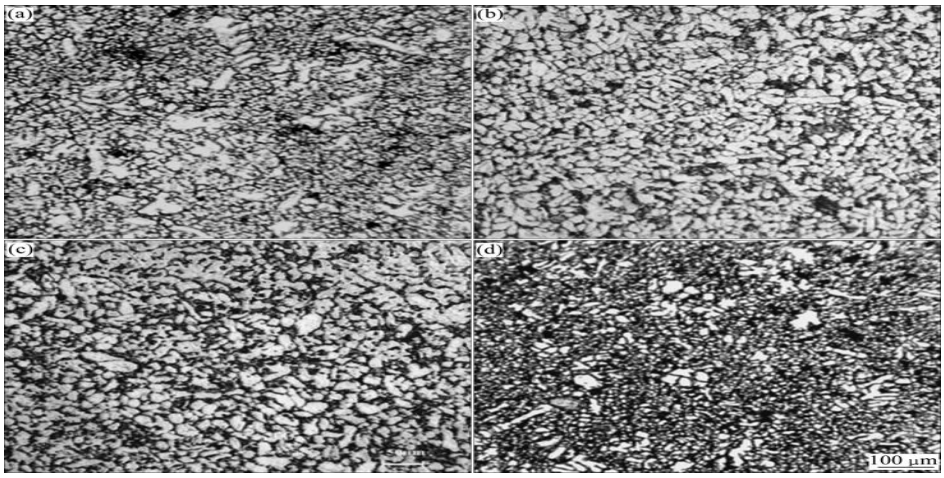

Figure 2.6 Optical micrographs of the (a) AZ91, (b) AZ91-1Y-0.5Ca, (c) AZ91-1Y-1.0Ca, and (d) AZ91-1Y-1.5Ca alloys [32]

More work was reported with combined addition as listed in Table 2.2

Table 2.2 Effect of additions of Sr and other alloying elements to AZ91 alloy

No.	Paper	% Sr	Findings
(i)	Liu et al. [38] (Ce+Ca+Sr)	0.2	Due to the low weight percentage of Sr additions no new phase was formed.
(ii)	Nakaura et al. [36] (Ca+Sr)	0.07 0.11 0.22	By the addition of approximately 0.2%Sr, die castability is significantly improved and creep resistance and mechanical properties also increase.
(iii)	Ming et al. (Sb+Sr+Si) [39]	0.12	The addition of 0.12%Sr to AZ61-0.7Si alloy, changed the shape of chinese script Mg_2Si from coarse chinese script shape to fine granule of irregular polygon this gave better creep properties than 0.4% Sb addition.
(iv)	Lee et al. [27] (Y+Sr+Nd)	0.492	Alloying elements of Y, Sr, and Nd added to the AZ91 alloy effectively improve hardness and grain refinement, owing to the homogeneous distribution of fine dispersoids within the matrix. The grain-refining effect of these alloying elements increases, in order, with Y, Nd, and Sr additions.
(v)	Jing et al. (Ca +Sr) [40]	Sr=1.0 2.0 3.0	Creep properties of Mg-Al alloy with Sr addition showed improvement in creep resistance at the temperatures between 150 and 200°C and stresses level 50-80MPa. Significant improvement with the increase in wt% of strontium addition the higher creep resistance is obtained in alloys with 1%of Ca addition.

2.8 Novelty of the present work

Selection of Sb and Sr as alloying constituents was based on following premises:

(i) Many have tried to improve the creep properties using rare earth metals and other expensive alloys which restrict the extensive use of Mg alloy. The alternative to this has been searched by the researcher vigorously in the late years on of the alternative that has been found the Alkaline earth metal group like Ca and Sb. Ca and Sb addition refine and modify the morphology of β-phase which results in better mechanical properties. But the addition of Ca forms intermetallic Al_2Ca which tends to distribute reticularly along the cell boundaries which is dangerous for mechanical properties. On the other hand Sb tends to form needle shape Mg_3Sb_2 precipitates which is effective climb or recovery obstacles [30].

(ii) By addition of 0.5 % Sr to AZ91 grain size reduction of 82μm to 48μm can be achieved [31]. The grain refinement obtained is attributed to the modified precipitation behavior observed with Sr addition. With the Sr addition, it was found that more amounts of β-phase are precipitated along the grain boundary. Sr can also combine with Al to form Al_4Sr, which can decrease the amount of β-phase [28].

(iii) Combined addition of Sb and Sr is a more implicit way in which both Sr and Sb forms intermetallic precipitates with different constituents Mg and Al so that balancing the final composition and also combined addition of Sb and Sr has been never done before "**Novelty in this work**" so it is a very scholastic opportunity to study their combined effect on mechanical properties of Squeeze casted alloy.

(iv) Squeeze casting method was chosen because it results in lower porosity and can be welded and heat-treated. The lack of porosity can significantly improve the creep properties as porosity provides the point of stress concentration.

Chapter 3

EXPERIMENTAL PROCEDURE

3.1 Work plan

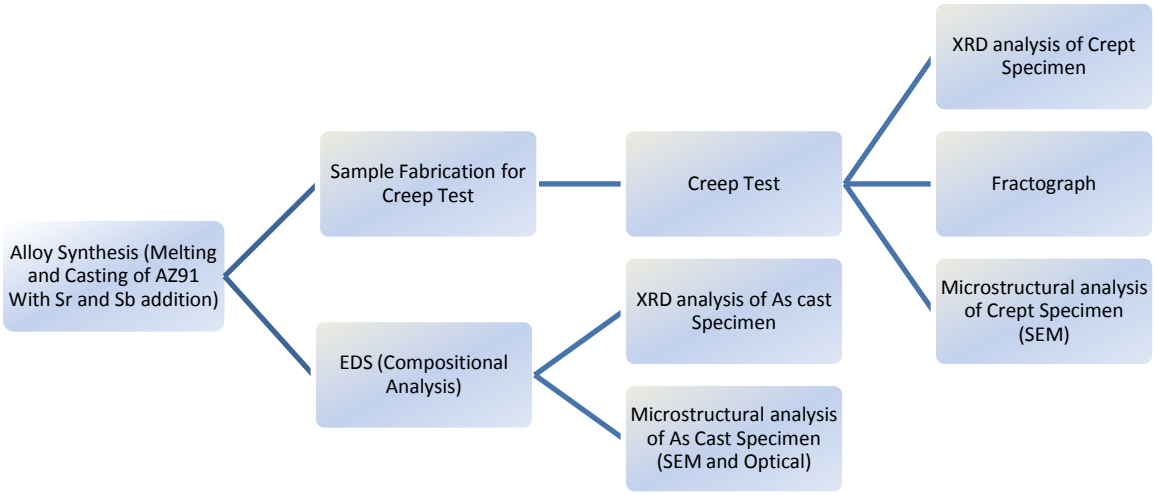

Figure 3.1 Detailed work plan

3.2 Fabrication of the alloys

AZ91 was selected as base metal, and final alloys were fabricated using following metals.

a) AZ91 ingots

b) Pure Sb flakes

c) Pure Sr flakes

d) Al-20% Sr master alloy

e) Pure Zn flakes

Materials required for casting

a) Cover gas (Ar and SF6)

b) Sand (to stop accidental fire)

3.2.1 Melting and casting

Casting of Mg alloys was done using bottom pouring type stir casting furnace that was also equipped with the hydraulic squeezer.

Figure 3.2 Bottom pouring stir casting furnace with squeeze casting facility

3.2.1.1 Squeeze casting of the AZ91 alloy

740 g of AZ91 die casted ingot was melted in a bottom pouring type stir casting furnace (Figure 3.2). The AZ91 was heated up to 720°C in the presence of the cover gas mixture of SF_6 and Ar. SF_6 and Ar gas was used to create a protective environment in the furnace during casting to stop the oxidization of the melt at high temperature. Cover gas SF_6 and Ar was first mixed in as Ar was flowed at pressure 18 Lb/in² for 50 sec and then SF_6 was flowed at pressure 7 Lb/in² for 3 sec, After that this mixture was used in the furnace as the cover gas. At temp 720°C the stirring of melt was done for 5 minute at RPM 442 after that pouring was done at temp 730°C of the melt. The squeeze casting of Alloy melt was done using a hydraulic press of 51 ton capacity in a steel mould preheated to temperature 220°C.

3.2.1.2 Squeeze casting of the AZY910 alloy

Casting of individual addition Sb Mg-alloy was carried out using AZ91 and Sb (purity 99.9%) granules. 1.5 wt% Sb was added to achieve target composition of 0.5wt% in the alloy. Preheated (325^0C) Sb added to the melt at temperature 680^0C. At temp 720^0C, the melt was stirred for 5 minute at RPM 442. Stirring was stopped after 5 minutes so that the impurity gets settled in the bottom before pouring. The squeeze casting of Alloy melt was done using a hydraulic press of 51 ton capacity in preheated (220^0C) steel mold (Figure 3.3). The flow chart for similar casting process for addition of Sb and Ca has been reported [33].

Figure 3.3 Squeeze cast AZY910 alloy

3.2.1.3 Squeeze casting of the AZJ910 and AZYJ9100 alloys

Sr was added individually in AZ91 following the same process except Sr was not preheated before mixing because of its high oxidizing tendency. Sr and Sb were added combinedly in AZ91 at same temperature and conditions. Master alloy Al+20%Sr and preheated Sb (purity 99.9%) granules were used for the combined addition casting. All the other process was followed as it was described in section 3.2.1.2.

3.3 Chemical analysis of the fabricated alloys

EDX analysis of all casted samples was done to determine the achieved composition. The EDX was conducted using Nova Nano 43 FEG-SEM. The bulk EDX of 5 different section of each alloy was taken, and an average was calculated.

Table 3.1 Results of bulk EDX analysis from the AZY910 alloy

Element	Wt %
MgK	68.48
AlK	29.52
SbL	00.36
ZnK	01.64

Element	Wt %
MgK	89.80
AlK	09.35
SbL	00.52
ZnK	00.33

Element	Wt %
MgK	89.83
AlK	08.14
SbL	00.78
ZnK	01.26

Element	Wt %
MgK	94.49
AlK	03.78
SbL	00.80
ZnK	00.93

Element	Wt %
MgK	89.69
AlK	09.04
SbL	00.40
ZnK	00.87

Table 3.2 Results of bulk EDX analysis from the AZJ910 alloy

Element	Wt %
O K	04.87
MgK	90.47
AlK	03.72
SrL	00.33
ZnK	00.59

Element	Wt %
O K	02.69
MgK	89.01
AlK	06.56
SrL	00.46
ZnK	01.28

Element	Wt %
O K	03.00
MgK	83.43
AlK	12.12
SrL	00.18
ZnK	01.27

Element	Wt %
O K	02.03
MgK	86.19
AlK	10.43
SrL	00.30
ZnK	01.04

Element	Wt %
O K	01.05
MgK	62.27
AlK	34.66
SrL	00.17
ZnK	01.85

Table 3.3 Results of bulk EDX analysis from the AZJY910 alloy

Element	Wt %
O K	03.70
MgK	63.92
AlK	28.41
SrL	00.54
SbL	00.50
FeK	00.28
ZnK	02.65

Element	*Wt %*
O K	03.93
MgK	90.20
AlK	03.46
SrL	00.43
SbL	00.54
FeK	00.46
ZnK	00.99

Element	Wt %
O K	02.23
MgK	61.60
AlK	31.50
SrL	00.19
SbL	00.63
FeK	00.60
ZnK	03.25

Element	Wt %
O K	01.98
MgK	84.69
AlK	12.05
SrL	00.27
SbL	00.25
FeK	00.07
ZnK	00.68

The achieved composition of all the fabricated alloys was in good agreement with the targeted composition as shown in Table 3.3.

Table 3.4 Target compositions, achieved compositions and corresponding alloy designations of squeeze-cast alloys

Target composition	Achieved composition	Alloy designation
AZ91D	AZ91D	AZ91
AZ91D-0.3Sr	AZ91D-0.288Sr	AZJ910
AZ91D-0.5Sb	AZ91D-0.572Sb	AZY910
AZ91D-0.3Sr-0.5Sb	AZ91D-0.356Sr-0.48Sb	AZJY9100

3.4 Creep test

The creep test specimen was fabricated from the squeeze casted alloys. The dimension of Sample for the test was formulated in accordance with ASTM E139 (Figure 3.4).

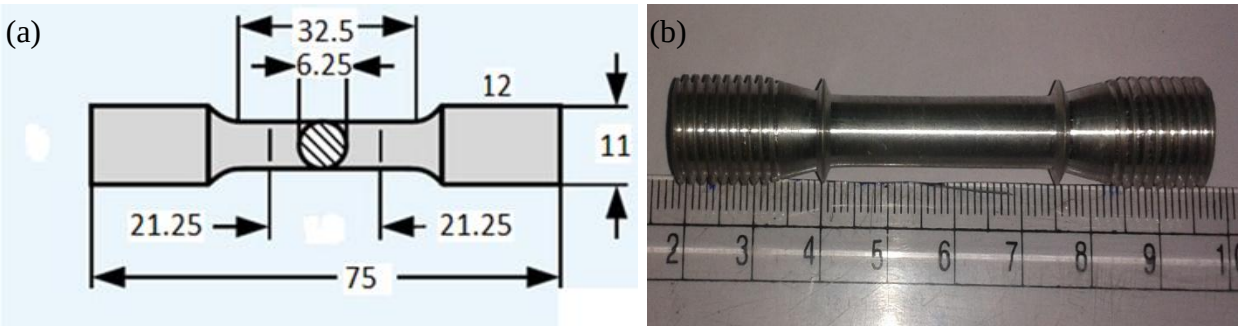

Figure 3.4 (a) Schematic of the creep test specimen, and (b) machined creep test specimen

Creep tests were performed on squeeze cast specimens using Mayes high temperature creep testing machine (Figure 3.5). Constant load creep rupture tests were conducted at a load of 70MPa at temperatures 175±2°C. The results of creep tests were based on the better of two test results for each alloy. The specimen deformation was measured through the attached extensometer on the specimen ridges. The specimen change in deformation get transferred from extensometer to two set of calibrated linear variable differential transducer (LVDT) mounted outside the furnace, and it was measured in volts. The strain was calculated from an average of two LVDT readings.

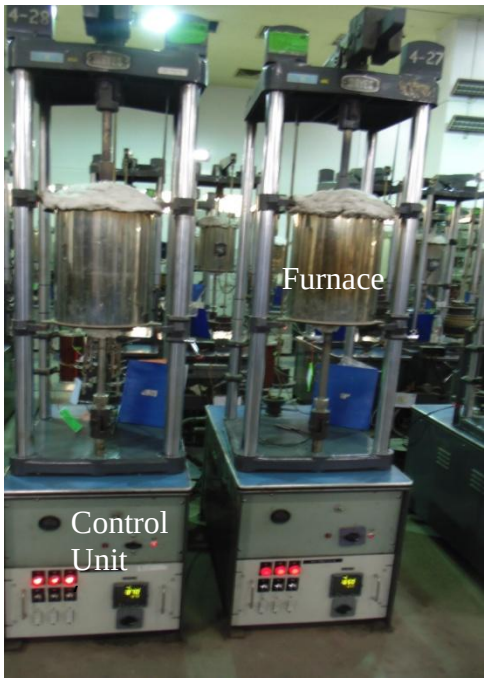

Figure 3.5 Photograph of the creep testing machines

3.5 Microstructural characterization

3.5.1 X-ray diffraction (XRD)

Phase analysis was carried out using XRD in D8 Discover Bruker XRD Diffractometer employing CuKα radiation in the diffraction angle (2θ) range from 10^{o} to 90^{o} to identify and analyze the phases in all alloys in as cast condition. The presence of intermetallic in alloy system was confirmed using XRD. The creep tested specimens were also analyzed by XRD to assess the stability of intermetallics during the creep.

3.5.2 Optical microscopy

Initially the samples (l5/5 mm rectangular sample) were polished using emery paper of 600, 1000, 2000 grits. Wax was used on the surface of emery paper to avoid the deep scratches.

After paper polishing, sample was polished on rotating disc with Beuler proprietary cloth using the diamond paste of 9, 6, 1, 0.1μm. Brasso was used as coolant so that the sample does not become too hot. Polishing was done by holding the specimen gently against the cloth to avoid the scratched as Mg is a very soft material. The diamond polishing was followed by 2 minute colloidal (SiO_2-0.01μm) polishing. After polishing, specimens were cleaned in the ultrasonic cleaner using ethanol. The specimens were etched using acetic picral (Acetic acid-2.5ml, picric acid-1.5g, ethanol-25ml, distill water-5ml). The etchant was aged for 30 minutes before use. The optical image was taken using LEICA DFC 295 optical microscope. Several images were taken from the different position using different magnification. The Leica MW software was used for calculation of grain size. The volume fraction of β- $Mg_{17}Al_{12}$ was calculated using Image J software.

3.5.3 Scanning electron microscopy

The precipitation analysis in all specimens was done using FEG-SEM. The chemical composition of all the precipitates was analyzed using EDS. SEM works at an accelerating voltage of 15-30KeV. The same specimens used in the optical analysis were also used for SEM. The specimen was cleaned after etching in the ultrasonic cleaner using ethanol. All the as cast specimens were analyzed in SEM, and different micrographs were taken at different magnification citing precipitation. EDS line scan was conducted to analyze the super saturated α-Mg with Al across the β- $Mg_{17}Al_{12}$ on grain boundary that causes the dynamic precipitation during creep. EDS Elemental mapping was done to see the distribution of elements. Creep tested specimen was also analyzed to see the creep cavity formation and effects of intermetallics on it.

Chapter 4

RESULTS AND DISCUSSION

4.1 Microstructural characterization

4.1.1 Phase analysis using XRD

The presences of different intermetallics were confirmed by XRD analysis. The diffraction pattern in the range of 20-90° (2θ) was obtained for all the as cast specimen (Figure 4.1).

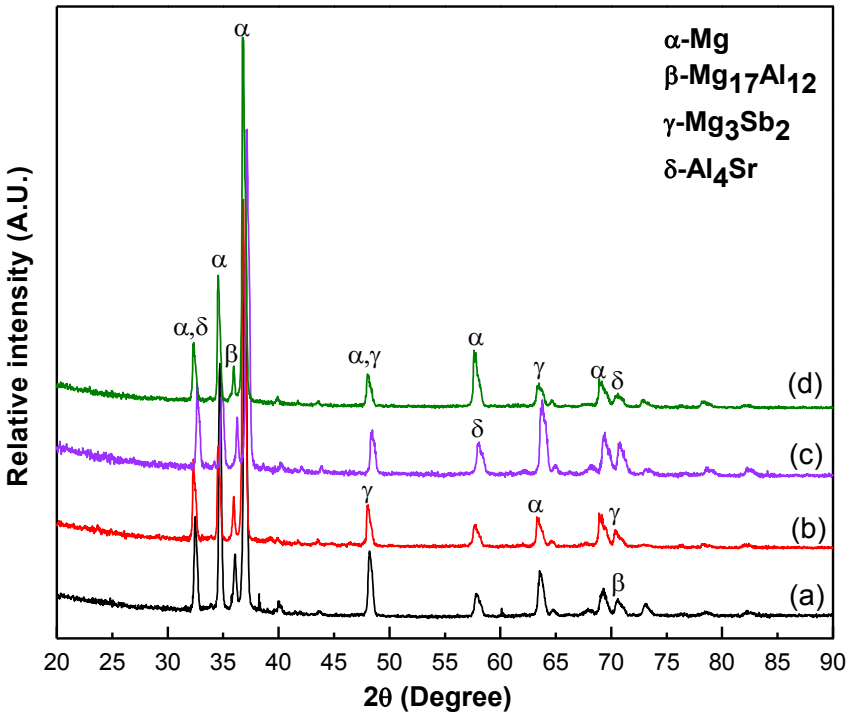

Figure 4.1 XRD patterns of the squeeze-cast (a) AZ91D, (b) AZY910, (c) AZJ910, and (d) AZJY9100 alloys

XRD pattern of alloys Peak consists of primary Mg (α-Mg) and β-$Mg_{17}Al_{12}$. Along with α peak peaks of Mg_3Sb_2 in AZY910 and AZJY9100, the peak of Al_4Sr in AZJ910 and AZJY9100 were also observed. The low intensity of Al_4Sr peak corresponds with low amount of Sr added. The decrease in intensity of peaks of the β-$Mg_{17}Al_{12}$ in alloys AZ91, AZY910, AZJ910, AZJY9100 successively confirm the decrease in its volume fraction due to grain refining by Sr and Sb.

4.1.2 Optical micrographs

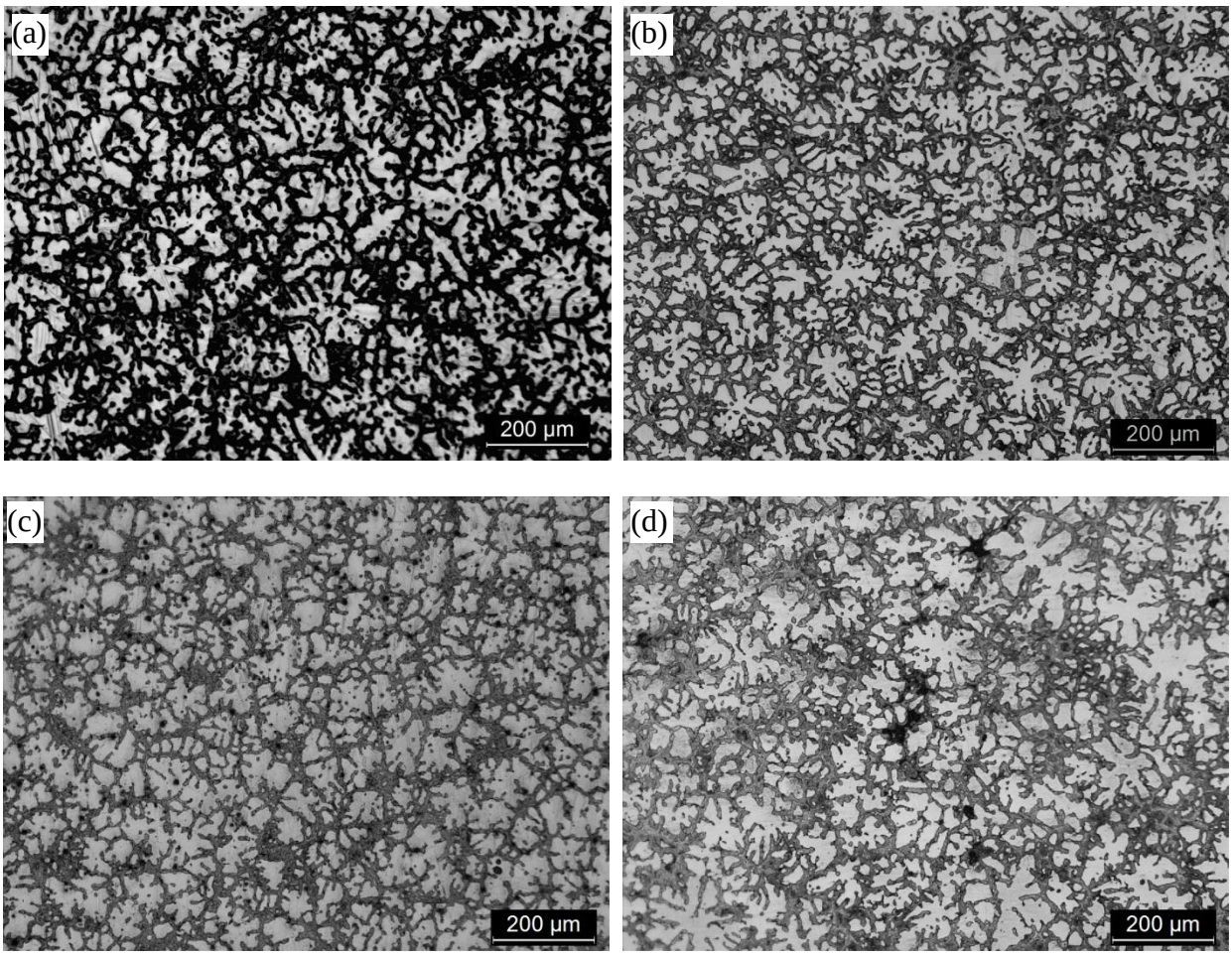

Figure 4.2 Optical micrographs of the squeeze-cast (a) AZ91D, (b) AZJ910, (c) AZY910, and (d) AZJY9100 alloys

Figure 4.2 (a-d) is showing the optical micrograph of all squeeze casted alloys. The difference in their microstructure is clearly visible. β-$Mg_{17}Al_{12}$ intermetallics solidified as a massive phase at the grain boundary because of higher cooling rate during squeeze casting. The addition of Sb and Sr to the AZ91 resulted in the decrease in the cell size of β-$Mg_{17}Al_{12}$ at grain boundary causing a decrease in its volume fraction (Table 4.1). Grain refinement due to Sr and Sb could be attributed to the constitutional super cooling. Sr and Sb provide constitutional super cooling on the solidification front which stops the growth [34].

Table 4.1 Grain size and volume fraction of the β-$Mg_{17}Al_{12}$ phase of the alloys

Alloy designation	Volume fraction of β-$Mg_{17}Al_{12}$ (%)	Calculated grain size (μm)
AZ91	13.85±0.13	66
AZY910	11.19±1.5	43
AZJ910	8.56±1.01	38
AZJY9100	8.37±0.4	33

Grain refining due to the addition of Sb is less prominent than Sr addition mainly because Sb has more tendency to form intermetallic. Lee et al. [27] (1997) and Hirai et al. 2005 [28] found similar grain size refining by Sr addition.

4.1.3 SEM micrographs

The addition of Sb and Sr causes the precipitation of intermetallics other than β- $Mg_{17}Al_{12}$ in the alloys AZY910, AZJ910 and AZJY9100. These intermetallics have very high thermal stability. The presence of these was confirmed through XRD in section 4.1.1. The composition of these intermetallics was confirmed using EDS in SEM. The micrograph shows the presence of these intermetallics on the grain boundary (Figure 4.3). Thermally stable intermetallic was found to be Mg_3Sb_2 with M.P. 1228°C and Al_4Sr with M.P 1040°C. The precipitation of eutectic β-$Mg_{17}Al_{12}$ along the grain boundary with many small α-Mg islands in between is called partial divorced eutectic (Figure 4.3). The continuous precipitation of β-$Mg_{17}Al_{12}$ did not take place as in the case of die casted alloy because of higher cooling rate (Figure 4.3). High solidification rate forms a supersaturated solid solution of Al in α-Mg along the grain boundary (Figure 4.4). The sharp decrease in Al wt% across the precipitate β-$Mg_{17}Al_{12}$ confirms the presence of α-Mg Island. This supersaturated α-Mg plays a major role during the creep. The interlamellar discontinuous precipitation of β-$Mg_{17}Al_{12}$ was not formed in these squeeze casted alloy as it has been reported in the case of die casting [20-30].

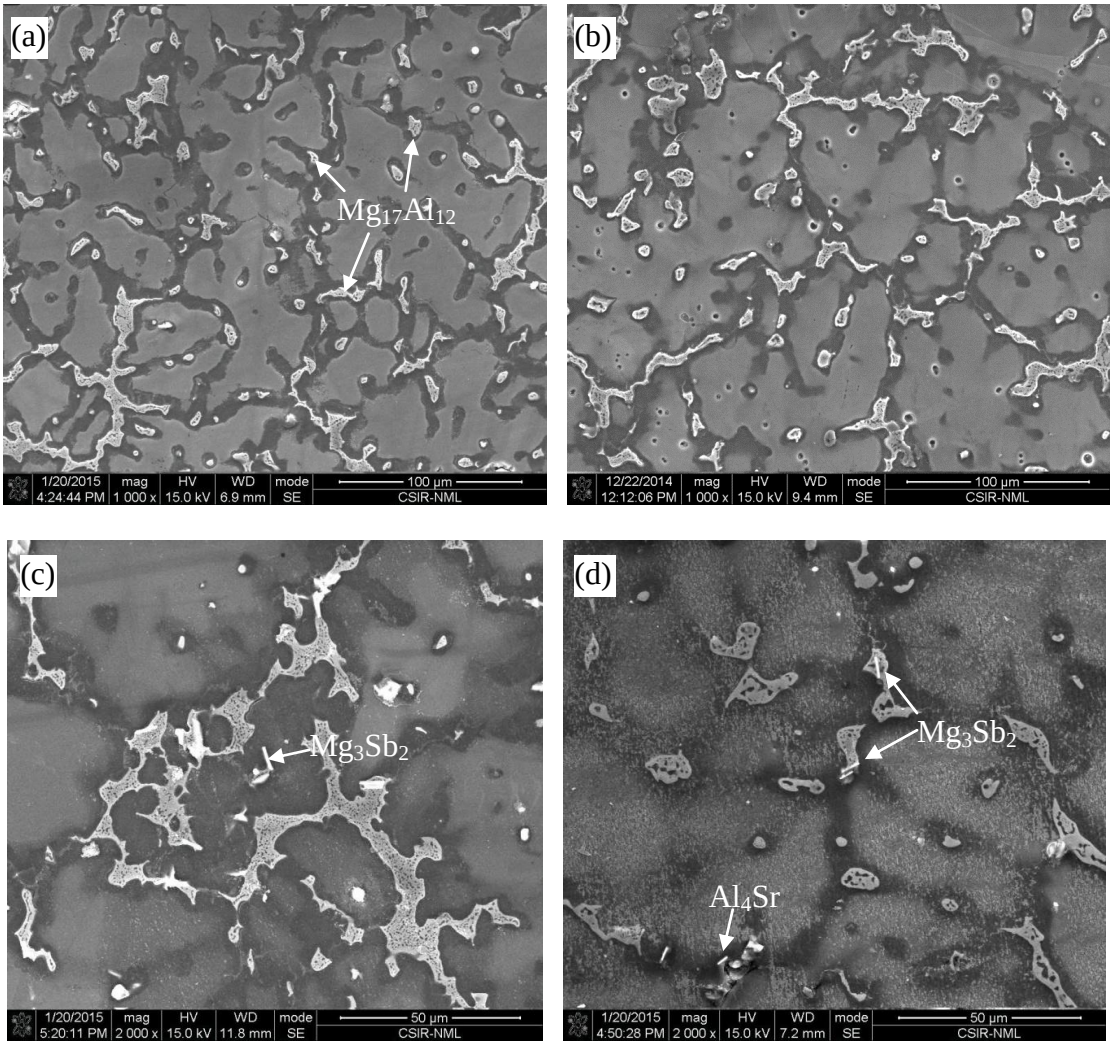

Figure 4.3 SEM micrographs of the squeeze-cast (a) AZ91D, (b) AZJ910, (c) AZY910, and (d) AZJY9100 alloys

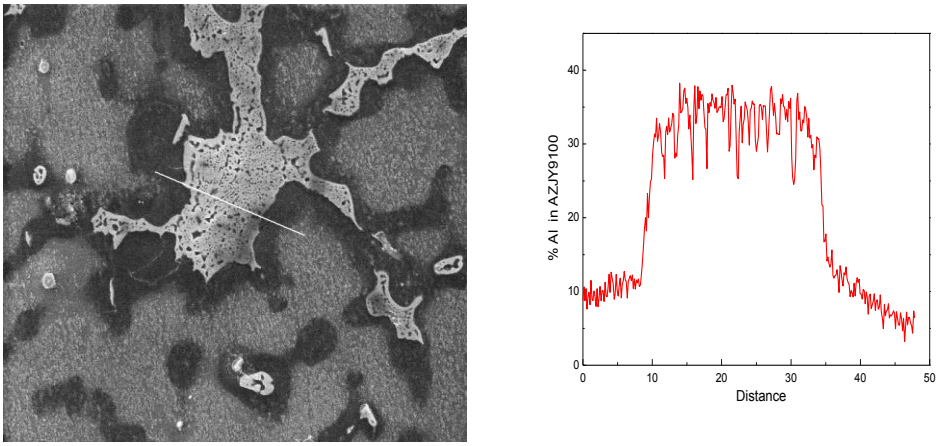

Figure 4.4 Variation of Al content (wt%) across the β-$Mg_{17}Al_{12}$ phase present along the grain boundaries

EDS elemental mapping of alloys were conducted in order to see the distribution of all the elements (Figure 4.5). The Figure 4.5 shows the presence of Al largely along the grain boundary as it forms intermetallic β-$Mg_{17}Al_{12}$ along the grain boundary. Other elements Zn, Sb, and Mn are evenly distributed along the grain boundary, which might be because they stopped the inward precipitation of β-$Mg_{17}Al_{12}$ in α-Mg by providing supercooling on solidification front.

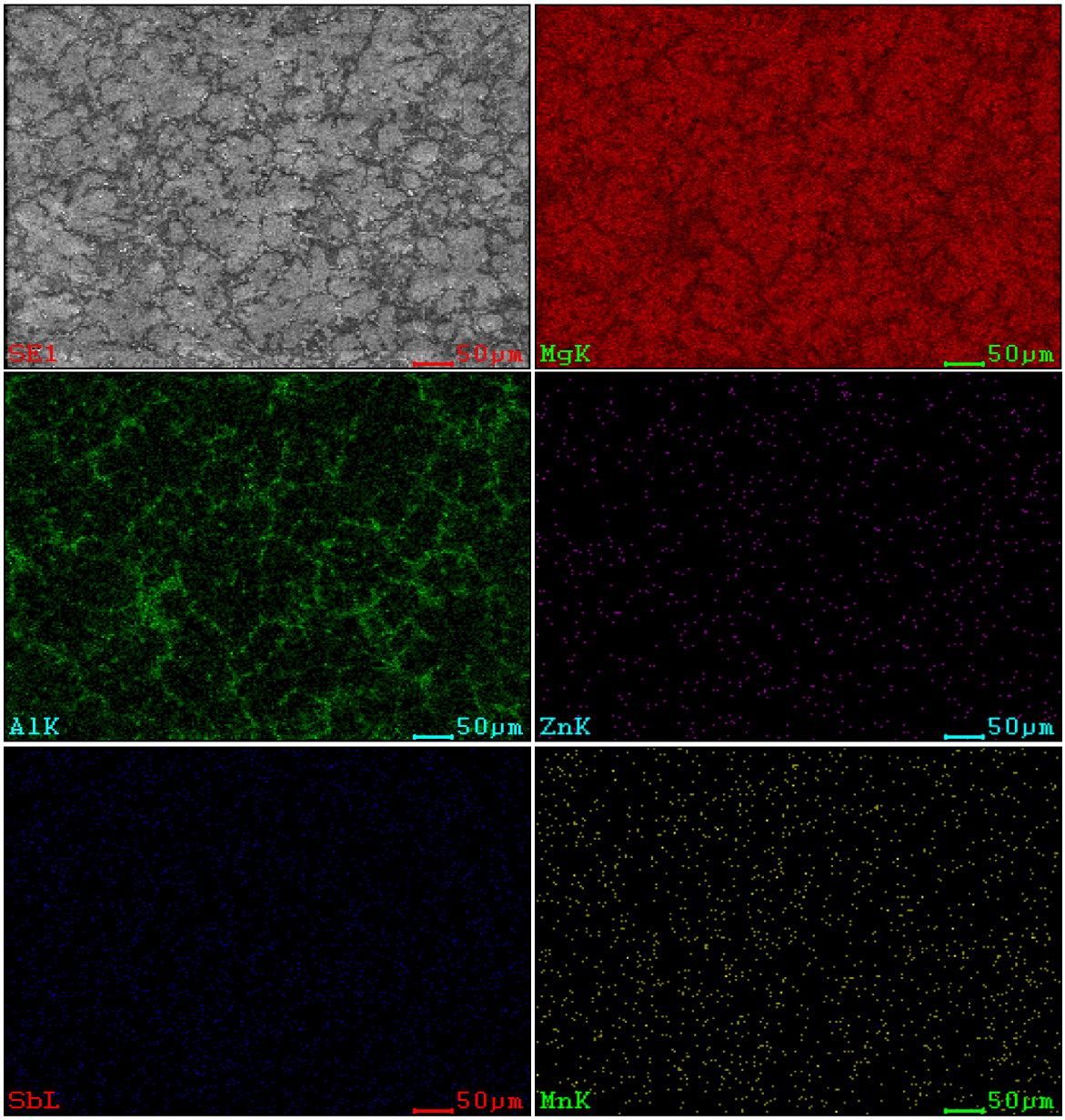

Figure 4.5 EDS elemental mapping taken from the AZJY9100 alloy for Mg, Al, Zn, Sb and Mn

4.2 Results of creep tests

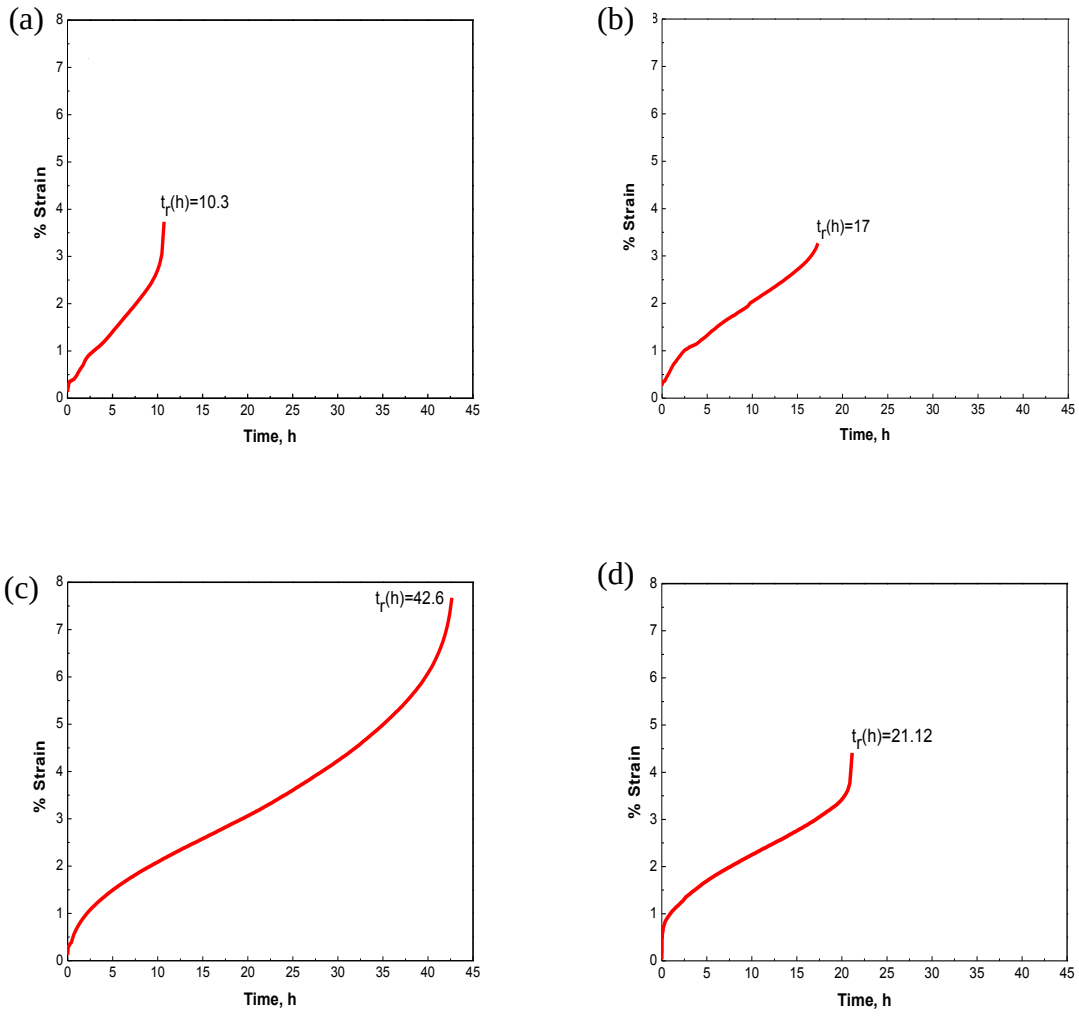

Figure 4.6 Creep curves of the (a) AZ91, (b) AZJ910, (c) AZY910 and (d) AZJY9100 Alloys tested at 70 MPa and 175°C

The specimens were tested at a stress level of 70 MPa and temperature 175°C till fracture. At 70 MPa Mg alloys show creep even at room temperature. Figure 4.6 (a) shows the creep curve of base alloy AZ91. The alloy is only showing tertiary creep region because of high stress and temperature. The creep was mostly controlled by grain boundary sliding mechanism [4].

Alloy AZJ910 is showing very small secondary creep region. AZJ910 is having better creep properties compared to base alloy AZ91 (Figure 4.6 (b)).

The reason behind this is the decrease in the amount of soft phase and the decrease in its cell size that reduced the rate of grain boundary sliding. The effect of intermetallic in the pinning of the grain boundary is not effective because Al_4Sr formed in small quantity owing to wt% Sr added. Alloy AZY910 showed larger improvement in creep resistance compared to other alloys. The reason behind this could be the presence of thermally stable Mg_3Sb_2, which pins the grain boundary very effectively [25]. But this fails to explain the low creep life of AZJY9100 compared to AZY910 (Figure 4.7(a)). One of the explanations might be the presence of more supersaturated Al inside the α-Mg in AZJY9100 as it has the low amount of β-$Mg_{17}Al_{12}$ (Figure 4.4). The supersaturated α-Mg results in dynamic precipitation during creep [6]. It has been established that discontinuous precipitation impairs the creep life of the AZ91 alloys [26]. The alloy AZJY91000 showed lowest steady state creep rate (Figure 4.7(b)) which suggests that initially Mg_3Sb_2 pinned successfully the grain boundary but it was unable to do in later stage due to coarsening of discontinuous precipitates β-$Mg_{17}Al_{12}$ [6]. Creep cavity started forming on the interface of supersaturated α-Mg Island and β-$Mg_{17}Al_{12}$ (Figure 4.7 (c)). Very small α-Mg Island was found on the massive β-$Mg_{17}Al_{12}$ which could be seen in Figure 4.4. The Al variation across the massive phase shown in Figure 4.4, the sharp decrease in wt % Al in between massive β-$Mg_{17}Al_{12}$ confirms the presence of very small supersaturated α-Mg. This α-Mg started growing by coalescence with each other during the creep (Figure 4.7); the coalescence of this island could be seen in Figure 4.7(d) which finally results in creep cavity formation on these [26]. Sr addition in AZJY9100 resulted in the higher amount of supersaturated Mg island which increased the α-β interface where creep cavity nucleates [27, 35]. This results in very sharp tertiary creep region in the alloy AZJY9100.

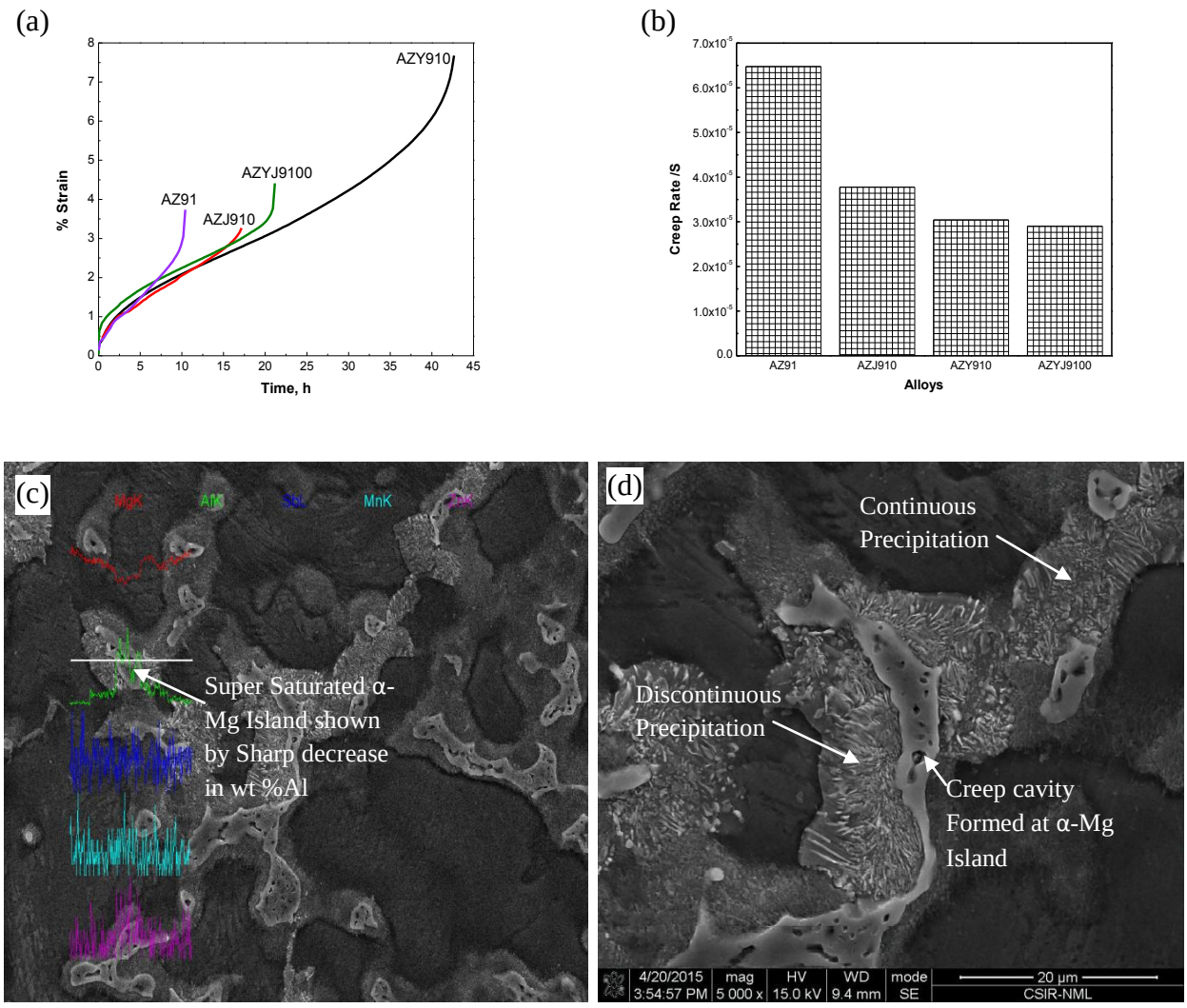

Figure 4.7 (a) Comparison of all the creep curves, (b) Steady state creep rate of the alloys; (c) results of line scan taken across β-$Mg_{17}Al_{12}$ phase in AZJY9100 alloy, and (d) SEM Micrograph of the creep cavity formed in the AZJY9100 alloy.

4.2.1 Phase analysis after creep tests

Figure 4.8 shows the XRD patterns obtained the AZJY9100 alloy before and after creep tests. The increase in peaks of β-$Mg_{17}Al_{12}$ after creep confirms its dynamic precipitation during creep. The peak intensity of Mg_4Al_4Sr decreases after creep, the metastablity of this phase that changes to Al_4Sr during creep, has been reported by [36].

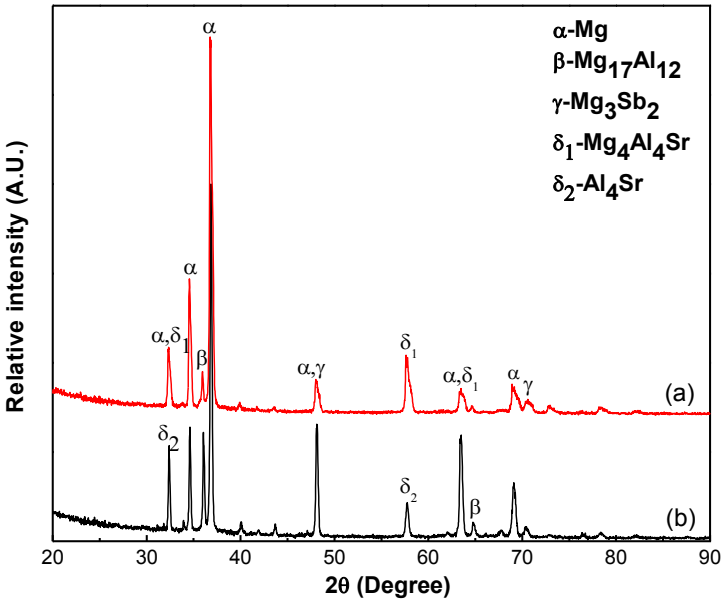

Figure 4.8 XRD patterns of the (a) as-cast, and (b) creep tested AZJY9100 alloy

No change in intensity of the Mg_3Sb_2 peak after creep test that confirms its stability at high temperature [25]. The presence of Mg_3Sb_2 is seen in the creep tested AZJY9100 alloy.

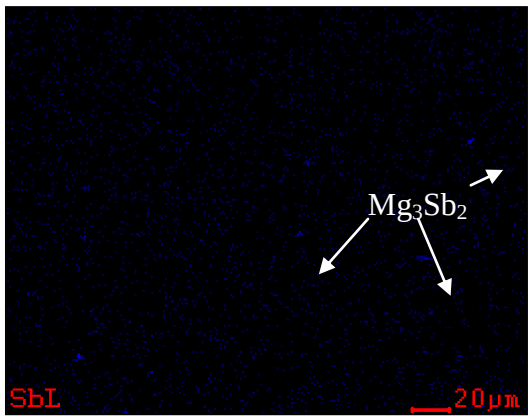

Figure 4.9 Elemental mapping taken from the AZJY9100 alloy showing Sb distribution

4.3 Fractography

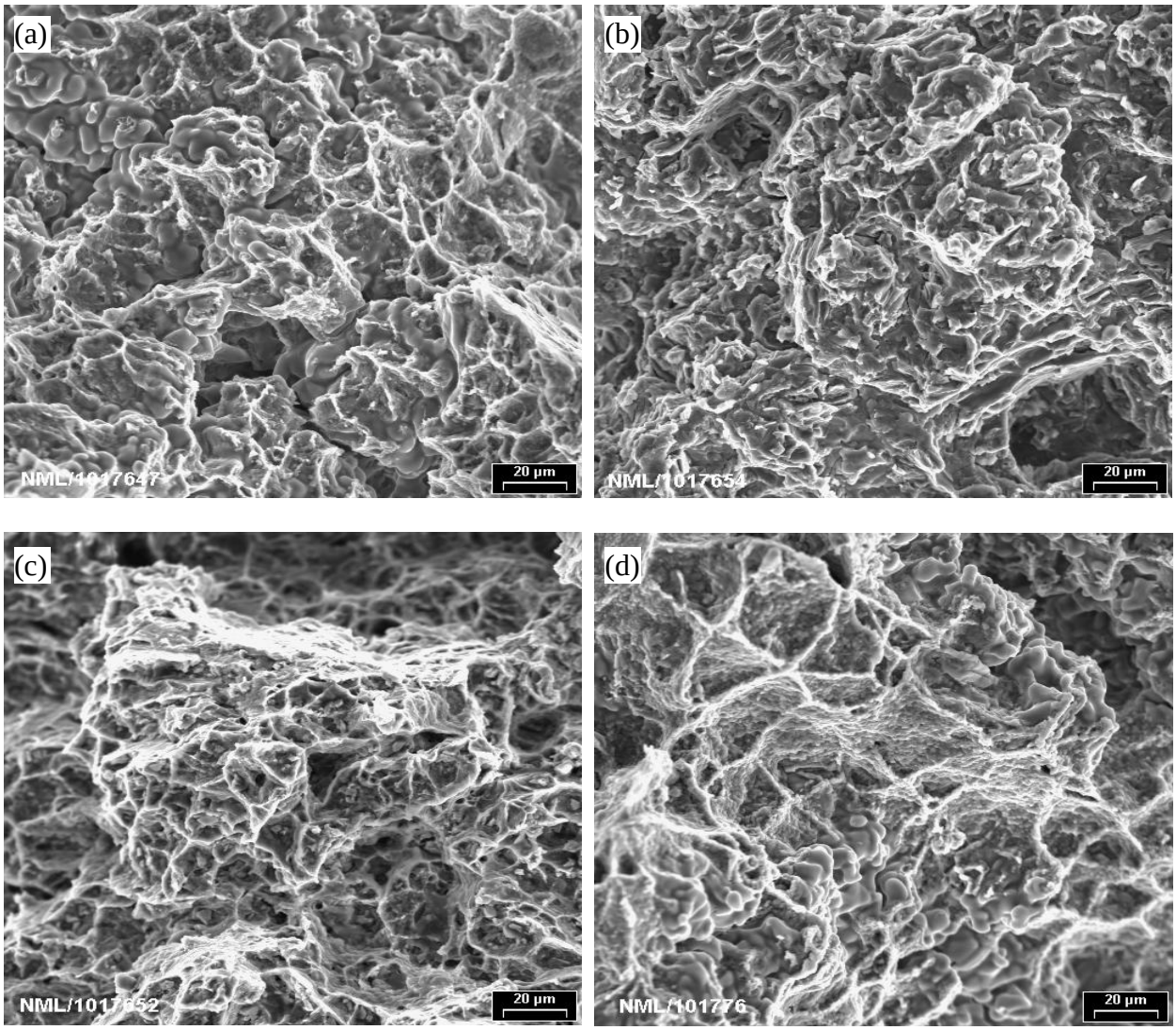

Figure 4.10 Fractographs of the creep tested (a) AZ91, (b) AZJ910, (c) AZY910, and (d) AZJY9100 alloys

Figure 4.10 shows the fracture surface of alloys AZ91, AZJ910, AZY910, and AZJY9100 creep tested at 70 MPa stress and 175°C temperature. Coalescence of the cavity by the faster rate at high temperature resulted in larger cavity in AZ91 alloy; it also have bigger grain size than other alloys [37]. The alloy AZJ910 shows brittle intergranular fracture as the brittle β-$Mg_{17}Al_{12}$ phase is distributed along the grain boundary and Al_4Sr was unable to pin G.B. effectively.

The higher ductility was found in alloy AZY910 and AZJY9100 because of the presence of Mg_3Sb_2 phase on grain boundary that hindered the intergranular fracture. The ductility was found to be lower in AZJY9100 because, after coarsening of dynamic β-$Mg_{17}Al_{12}$ precipitates Mg_3Sb_2 was unable to pin the grain boundary. It can be deduced as intergranular fracture is more prevalent in AZJY9100.

Chapter 5

CONCLUSIONS

5.1 Conclusions

The effects of combined additions of Sr and Sb on the microstructure and creep behaviour of the AZ91 alloy fabricated by squeeze-casting were investigated. For comparison, the same was also studied on the squeeze-cast base AZ91 alloy as well as AZ91 alloy with individual additions of Sr and Sb. The following conclusions are drawn:

i. Individual and combined additions of Sr (0.3%) and Sb (0.5%) (wt%) to AZ91 alloy refined the grains significantly and also suppressed the formation of β-$Mg_{17}Al_{12}$ phase, which resulted better creep resistance of all the modified AZ91 alloys.

ii. The AZ91-based alloys with individual as well as combined additions exhibited better creep resistance than that of the base AZ91 alloy. The AZY910 alloy revealed the highest creep life and the AZJY9100 alloy showed the lowest steady state creep rate.

iii. The Sr addition had more impact on the refinement and suppression of the β-$Mg_{17}Al_{12}$ phase. The supersaturated α-Mg island formed on the massive β-$Mg_{17}Al_{12}$ phase present along the grain boundaries of the AZJ910 and AZJY9100 alloys. Nucleation of the creep cavities took place at the α-Mg resulting early fracture of both the alloys.

5.2 Future scope of work

The combined Addition resulted in lowest steady state creep rate but the creep life did not improved significantly. This future scope of this work is to improve the creep life of alloy AZJY9100. One of the methods could be the introduction of dislocations in the alloy (rolling) that will act as a nucleation site for continuous precipitation, which could improve creep life by extending secondary creep region.

Chapter 5

REFERENCES

[1] Lou A., Journal of Materials, 54 (2002) 42-48.

[2] Dieter G.E., Mechanical Metallurgy, Mc Graw Hill, New Delhi 2013.

[3] Dahle A. K., St John D. H. and Dunlop G. L., Material Science Forum 24 (2000) 159-167.

[4] Yang Z., Liz J.P., Acta Metallurgica Sinica Science 21 (2008) 313-328.

[5] Regev M., Aghoin E., Metallurgical and Materials Transaction A 32 (2001) 1335-1345.

[6] Blum W., Watzinger B., Advance Engineering Material 2 (2000) 349-355.

[7] Amberger D., Eisen lohrb P., Gokena M., Materials Science and Engineering A 510-511 (2009) 398-402.

[8] Franzese O., OAK Ridge National Laboratory (2011).

[9] <http://www.ipcc.ch> [Last accessed 28 April 2015].

[10] Magnesium Electron Limited, Magnesium Alloy Database

[11] Pekgureyuz M.O., Material Science Forum 350-351 (2000) 131-140.

[12] Luo Z. D. Song D. Y., Journal of Alloys and Compounds 230 (1995) 109-114.

[13] Suzuki M., Sato H., Material Science Engineering 252A (1998) 248-255.

[14] Maruyama K., Suzuki M., Sato H., Metallurgical and Materials Transaction A 33 (2002) 875-882.

[15] Abachi P., Masaudi A., Material Science and Engineering A 435-439 (2006) 653-657.

[16] Polmear: Proc. Magnesium Alloys and Their Application, B. L. Mordike and Hehmaan F., Germany (1992) 201-212.

[17] Bakke P., Westengen H., Advance Engineering Materials 5 (2003) 879-885.

[18] Qudong W., Wienzhou C., Journal of Material Science 36 (2001) 3035-3040.

[19] Lin L., Wang F., Yang L, Metallurgical and Materials Transaction A 528 (2011) 1261-1267.

[20] Luo A. A., Michael P., Metallurgical and Materials Transaction A 33 (2002) 567-574.

[21] Nami B., Shabestari S. G., Razari H., Material Science and Engineering A 528 (2011) 1261-1267.

[22] Amberger D., Elsenlohr P., Goken M., Material Science and Engineering 510-511 (2009) 398-402.

[23] Guangyin X., Yangshan S., Material Science Engineering A 308 (2001) 38-44.

[24] Wang Q., Chen W., Ding W., Metallurgical and Materials Transaction A 32 (2001) 787-794.

[25] Guanzyian Y., Yangshan S., Scripta Materialia 43 (2000) 1009-1013.

[26] Srinivasan A., Ajith Kumar K. K., Procedia Engineering 55 (2013) 109-113.

[27] Lee S., Lee S. H., Metallurgical Materials Transaction A 29 (1998) 1221-1235.

[28] Hirai K., Somekaw H., Material Science and Engineering A 403 (2005) 276-280.

[29] Nakura Y., Watanabe A., Material Transaction 47 (2006) 1031-1039.

[30] Srinivasan A., Swaminathan J., Material Science and Engineering A 455 (2008) 86-91.

[31] Srinivasan A., Pillai U. T. S., International Symposium of Research Student on Material Science and Engineering (2004).

[32] Feng W., Yeue W., Trans Non Ferrous Material Society China 20 (2010) 311-317.

[33] Bankoti A. K. S., Mondal A. K., Materials Science and Engineering A 626 (2015) 186–194.

[34] John D. H., Metallica Materials Transaction A 36 (2005) 1671-1679.

[35] Brittle C. J., Gibson M. A., Advance Engineering Material 5 (2003) 859-865.

[36] Nakaura Y., Watanabe A., Materials Transactions 47 (2006) 1031-1039.

[37] Poddar P., Ray A. K., Materials Science and Engineering A 45 (2012) 103-110.

[38] Liu S. F., Li B., Journal of Material Processing Technology 209 (2009) 3999-4004.

[39] Ming-bo Y., Fu-Sheng P., Trans Nonferrous Material Society China 19 (2009) 287-292.

[40] Jing B., Yangshan S., Material Science and Engineering A 419 (2006) 181-188.